Scalar meson in dynamical and partially quenched two-flavor QCD: Lattice results and chiral loops

S. Prelovsek,[1,2] C. Dawson,[3] T. Izubuchi,[3,4] K. Orginos,[5] and A. Soni[6]

[1]*Department of Physics, University of Ljubljana, Jadranska 19, 1000 Ljubljana, Slovenia*
[2]*Institute Jozef Stefan, Jamova 39, 1000 Ljubljana, Slovenia*
[3]*RIKEN-BNL Research Center, Brookhaven National Laboratory, Upton, New York 11973, USA*
[4]*Institute of Theoretical Physics, Kanazawa University, Ishikawa 920-1192, Japan*
[5]*Center for Theoretical Physics, Laboratory for Nuclear Science and Department of Physics, MIT, Cambridge, Massachusetts 02139-4307, USA*
[6]*Physics Department, Brookhaven National Laboratory, Upton, New York 11973, USA*

(Received 16 August 2004; published 18 November 2004)

This is an exploratory study of the lightest nonsinglet scalar $q\bar{q}$ state on the lattice with two dynamical quarks. Domain wall fermions are used for both sea and valence quarks on a $16^3 \times 32$ lattice with an inverse lattice spacing of 1.7 GeV. We extract the scalar meson mass 1.58 ± 0.34 GeV from the exponential time dependence of the dynamical correlators with $m_{\rm val} = m_{\rm sea}$ and $N_f = 2$. Since this statistical error bar from dynamical correlators is rather large, we analyze also the partially quenched lattice correlators with $m_{\rm val} \neq m_{\rm sea}$. They are positive for $m_{\rm val} \geq m_{\rm sea}$ and negative for $m_{\rm val} < m_{\rm sea}$. In order to understand this striking effect of partial quenching, we derive the scalar correlator within the partially quenched chiral perturbation theory (ChPT) and find it describes lattice correlators well. The leading unphysical contribution in partially quenched ChPT comes from the exchange of the two pseudoscalar fields and is also positive for $m_{\rm val} \geq m_{\rm sea}$ and negative for $m_{\rm val} < m_{\rm sea}$ at large t. After the subtraction of this unphysical contribution from the partially quenched lattice correlators, the correlators are positive and exponentially falling. The resulting scalar meson mass 1.51 ± 0.19 GeV from the partially quenched correlators is consistent with the dynamical result and has an appreciably smaller error bar.

DOI: 10.1103/PhysRevD.70.094503 PACS numbers: 11.15.Ha, 12.38.Gc, 12.39.Fe

I. INTRODUCTION

Interest in the light scalar mesons has been renewed recently [1]. The existence of the scalar mesons above 1 GeV is well established experimentally and there are enough scalar states between 1 and 2 GeV to represent the scalar $q\bar{q}$ nonet [2]. The excess of one observed state in this region has been suggested as an indication for the glueball [3]. The lightest isotriplet state above 1 GeV is $a_0(1450)$. The only scalar states below 1 GeV, which are experimentally well established, are isotriplet $a_0(980)$ and isosinglet $f_0(980)$ [2]. The existence of the complete scalar $q\bar{q}$ nonet roughly below 1 GeV would require another isosinglet and two strange isodoublets. The experimental evidence for the existence of a broad isosinglet σ meson around 600 MeV is growing [2,4], while the existence of the strange isodoublet κ reported in [5] is even more controversial at present. This raises a question whether the lightest scalar $q\bar{q}$ states lie below 1 GeV or above 1 GeV. In the latter case, the observed scalar states below 1 GeV have to be interpreted as exotic states like $qq\bar{q}\bar{q}$ [6], $\pi\pi$ or $K\bar{K}$ molecules, etc.

In this paper we address the determination of the mass of the lightest scalar $q\bar{q}$ state with nonsinglet flavor structure (referred to as the a_0 meson [2]), the long-term goal being to relate this state to the observed resonance $a_0(1450)$ or $a_0(980)$. We determine the mass of the a_0 meson using a lattice simulation of dynamical QCD ($m_{\rm val} = m_{\rm sea}$) and partially quenched QCD ($m_{\rm val} \neq m_{\rm sea}$) with $N_f = 2$ degenerate sea quarks in both cases. Since our aim is the $q\bar{q}$ state composed of the light u and d quarks, we employ domain wall fermion (DWF) formalism, which has good chiral properties [7]. We comment also on the mass of the $s\bar{u}$ and $s\bar{d}$ scalar mesons.

While DWF formulation ought to be helpful in the long run, at present our numerical work has serious limitations. We are working with two dynamical flavors, which is not full QCD. Furthermore we have results only at one lattice spacing on a lattice box that is not very large and also quarks are relatively heavy. For these reasons, this is an exploratory work. These issues can of course be improved with more computing resources.

Before we introduce our work, we briefly review the recent lattice simulations of the light nonsinglet scalar states. We quote only the statistical error bars on masses since the continuum and infinite-volume extrapolations have not been performed in these simulations:

(i) *Fully quenched simulations of* $q\bar{q}$.—The quenched $q\bar{q}$ correlator in the chiral limit was simulated by Bardeen *et al.* [8,9] with Wilson fermions. The correlators were found to be nega-

tive at small quark masses, which was attributed to the similar mechanism as observed in the present partially quenched study. The effects of quenching were modeled using the quenched chiral perturbation theory and subtracted in order to extract the scalar meson mass $m_{a0} = 1.326(86)$ GeV [9].

The RBC Collaboration simulated nonsinglet and singlet scalar $q\bar{q}$ states with domain wall fermions [10]. The quenching effect, which leads to negative correlators at small quark masses, was subtracted as in [8,9]. The result is $m_{a0} = 1.43(10)$ GeV if only the leading chiral loop (one bubble) is taken into account, and $m_{a0} = 1.04(7)$ GeV if next-to-leading chiral corrections are included by resummation.[1]

Mixing of the glueball and $q\bar{q}$ was studied in [3]. The quark mass was around m_s and no attempt was made to go to the chiral limit.

(ii) *Dynamical simulations of* $q\bar{q}$.—The SCALAR Collaboration made an extensive simulation of the singlet $\bar{q}q$ state [11] and extracted also the mass of the nonsinglet state to be $m_{a0} \sim 1.8$ GeV at $m_\pi/m_\rho \sim 0.7$. They consider this estimate as an upper bound on the mass since they fitted the correlators at relatively low times, where contribution of the excited state might be sizable. UKQCD extracted $m_{a0} \sim 1.0(2)$ GeV from the dynamical and the partially quenched simulation of $q\bar{q}$ [12]. Since they simulated only $m_{\rm val} \geq m_{\rm sea}$, they did not observe the striking effect of partial quenching discussed below. For this reason, they were able to extract the scalar mass from the exponential time dependence.

MILC [13] simulated the $q\bar{q}$ state with three dynamical flavors and saw an indication for the intermediate state $\pi\eta$, since this state is lighter than the a_0 state at the lightest quark masses.

(iii) Alford and Jaffe reported an indication for the bound singlet and octet $qq\bar{q}\bar{q}$ states below 1 GeV [6].

All simulations above employed Wilson fermions, except for RBC and MILC simulations, which employed domain wall and staggered fermions, respectively.

The only simulation which employed chiral fermions to study light scalar mesons is the quenched simulation of RBC [10]. Chiral symmetry is expected to be particularly important for the singlet scalar meson σ, which is intimately connected with the chiral symmetry breaking. Good understanding of the nonsinglet correlator in the chiral limit is the first step toward the controlled study of the σ meson. As already mentioned, the present paper presents the dynamical simulation ($m_{\rm sea} = m_{\rm val}$) of the nonsinglet $q\bar{q}$ correlator with domain wall fermions. We also simulate partially quenched QCD with $m_{\rm val} \neq m_{\rm sea}$. Two degenerate sea quarks have the range of masses corresponding to $M_\pi \sim 500$–700 MeV [14]. The scalar correlators for $m_{\rm sea} = 0.02$ and $m_{\rm sea} = 0.03$ at various $m_{\rm val}$ are shown in Fig. 1. The correlators for $m_{\rm val} \geq m_{\rm sea}$ are positive and have more or less exponential time dependence. On the other hand, the correlators for $m_{\rm val} < m_{\rm sea}$ are negative due to a striking effect of partial quenching. We note that the point-point correlator should be positive definite in the dynamical QCD based on unitarity, which is broken in the partially quenched QCD. We derive the effect of partial quenching on the scalar correlator using the partially quenched chiral perturbation theory (PQChPT) [15] in a finite box. The leading unphysical effect is due to the exchange of the two pseudoscalar fields; it is represented by the bubble diagram in Fig. 3(b) (below) and has no unknown parameters. We show that the bubble diagram gives a positive contribution for $m_{\rm val} \geq m_{\rm sea}$ and a negative contribution for $m_{\rm val} < m_{\rm sea}$ at large time separations. We find that the negative lattice correlators with $m_{\rm val} < m_{\rm sea}$ are well described by the bubble contribution. This enables us to extract m_{a0} in the partially quenched simulation.

The remainder of this paper is organized as follows. The details about the lattice simulation are presented in Sec. II. The dynamical correlators are analyzed in Sec. III. The resulting error on the scalar mass is rather large, which motivates us to analyze also the partially quenched correlators. The partially quenched artifacts on the scalar correlator are derived within PQChPT in Sec. IV and used to analyze the partially quenched correlators in Sec. V. Section VI summarizes the conclusions on the mass of a_0 meson and briefly comments on mass of the κ resonance, while Sec. VII summarizes the general conclusions.

II. NUMERICAL SIMULATION

The RBC Collaboration has undertaken a large-scale simulation with $N_f = 2$ flavors of dynamical domain wall quarks with degenerate masses [14]. This is an improvement over the quenched simulations and represents an important step toward the simulation of QCD with three dynamical quarks of physical masses. The scalar correlators were calculated on the dynamical configurations with the volume $N_L^3 N_T = 16^3 32$ and a single lattice spacing, so we will not be able to extrapolate the scalar mass to the continuum and to the infinite volume in the present work. The configurations were generated using DBW2 gauge action

[1]The higher order chiral corrections $\mathcal{O}[M_\pi^2/(4\pi f)^2]$ have a smaller effect on the scalar mass in Refs. [8,9] since their value of the pseudoscalar decay constant f is larger than the physical value.

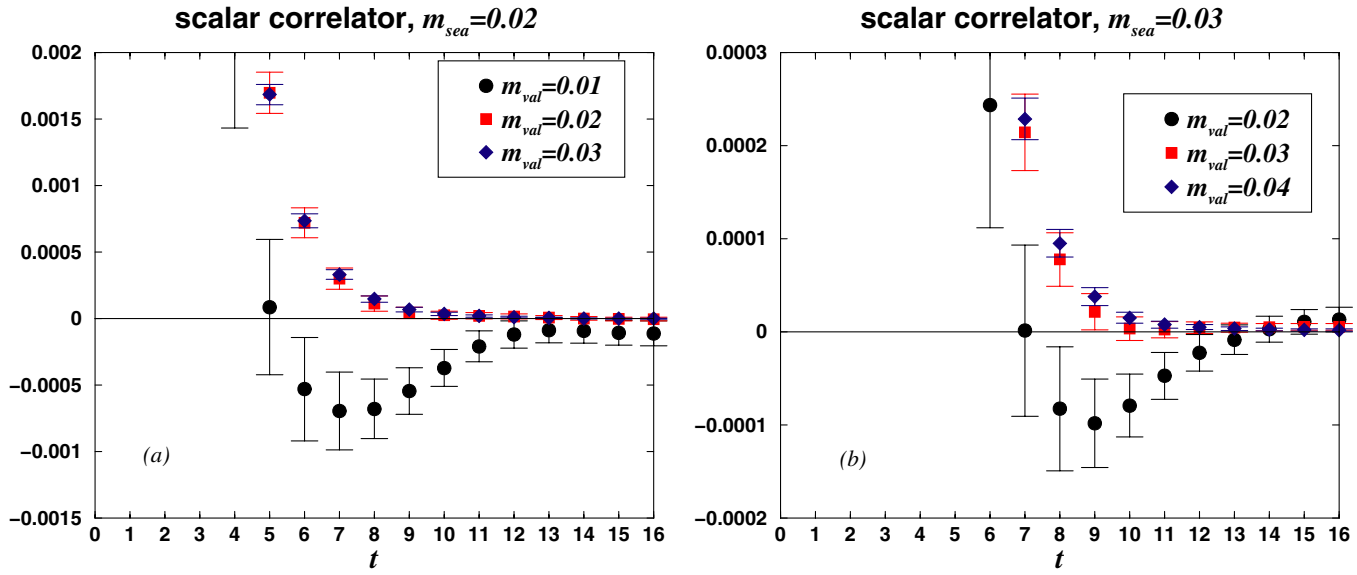

FIG. 1 (color online). The scalar correlators from lattice at (a) $m_{\mathrm{sea}} = 0.02$ and (b) $m_{\mathrm{sea}} = 0.03$ for various m_{val}.

[16][2] with $\beta = 0.80$ and domain wall fermion action [7] with $M_5 = 1.8$ and $L_s = 12$ (L_s is the extent in the fifth dimension) [14]. The separate evolutions were performed for three different bare sea-quark masses $m_{\mathrm{sea}} = 0.02, 0.03, 0.04$, which correspond approximately to $M_\pi \sim 500$–700 MeV. These quark masses are below the strange quark mass, whose bare value is estimated to be $m_s = 0.045(3)$ [14]. The measurements of the correlators were performed on configurations separated by 50 hybrid Monte Carlo trajectories. Dynamical domain wall fermions have good chiral properties even at finite L_s with the additive shift in the mass due to the residual chiral symmetry breaking, m_{res}, being approximately 0.0014 [14], much smaller than either the input sea or valence-quark masses. The inverse lattice spacing was determined from the ρ-meson mass and the preliminary result is $a^{-1} \approx 1.7$ GeV [14]. The current uncertainty of the lattice spacing has a small effect on the scalar mass; the uncertainty of the scalar meson mass in the present work is dominated by the statistical errors of the scalar correlators.

The scalar correlators were measured for the degenerate valence-quark masses $m_1 = m_2 \equiv m_{\mathrm{val}}$ in the range $m_{\mathrm{val}} = 0.01$–0.05. These valence-quark masses correspond approximately to $M_\pi \sim 380$–770 MeV [Fig. 4 (below)]. We used the point source and the point sink since the analysis of the correlators is based on the PQChPT, which predicts the magnitude of the partially quenched effects only for the point-point correlators. The point-point correlators with $p = 0$ were simulated via

$$\frac{1}{N_L^3} \sum_{\vec{x},\vec{x}',\vec{y}} \langle 0|\bar{q}(\vec{x}, t)\Gamma q(\vec{x}', t)\bar{q}(\vec{y}, 0)\Gamma q(\vec{y}, 0)|0\rangle,$$

with $\Gamma = I$ on the lattices with unfixed gauge. The average over the configurations with unfixed gauge gives the point-point correlator [18]

$$C_{pp} = \frac{1}{N_L^3} \sum_{\vec{x},\vec{y}} \langle 0|\bar{q}(\vec{x}, t)\Gamma q(\vec{x}, t)\bar{q}(\vec{y}, 0)\Gamma q(\vec{y}, 0)|0\rangle. \quad (1)$$

This method enabled us to calculate also the singlet scalar and singlet pseudoscalar correlators and to determine the hairpin insertion m_0.

The summary of the scalar and pseudoscalar correlators analyzed in the present paper is given in the Table I.

TABLE I. The summary of the scalar and pseudoscalar correlators analyzed in this work. All correlators are calculated at $V = 16^3 \times 32$, $a^{-1} \approx 1.7$ GeV, degenerate valence quarks, two degenerate sea quarks, point source, and point sink.

m_{sea}	m_{val}	Configurations
0.02	0.01–0.05	94
0.03	0.02–0.04	94
0.04	0.04	94

[2]DBW2 gauge action is known to break the reflection positivity of the transfer matrix [17], which is the counterpart of the unitarity for Euclidean lattice theory. Hence, there is a possibility that the negative value of the scalar correlator is partially caused by the complex eigenvalues of the transfer matrix. We concentrate our analysis at large time separation $t \geq 4$, where the negative contribution to the two-point function is expected to disappear. We perform the comparison between the full QCD and the (partially) quenched QCD with $m_{\mathrm{val}} < m_{\mathrm{sea}}$ using the same DBW2 gauge action and find negative scalar correlator only in the case of the (partially) quenched QCD.

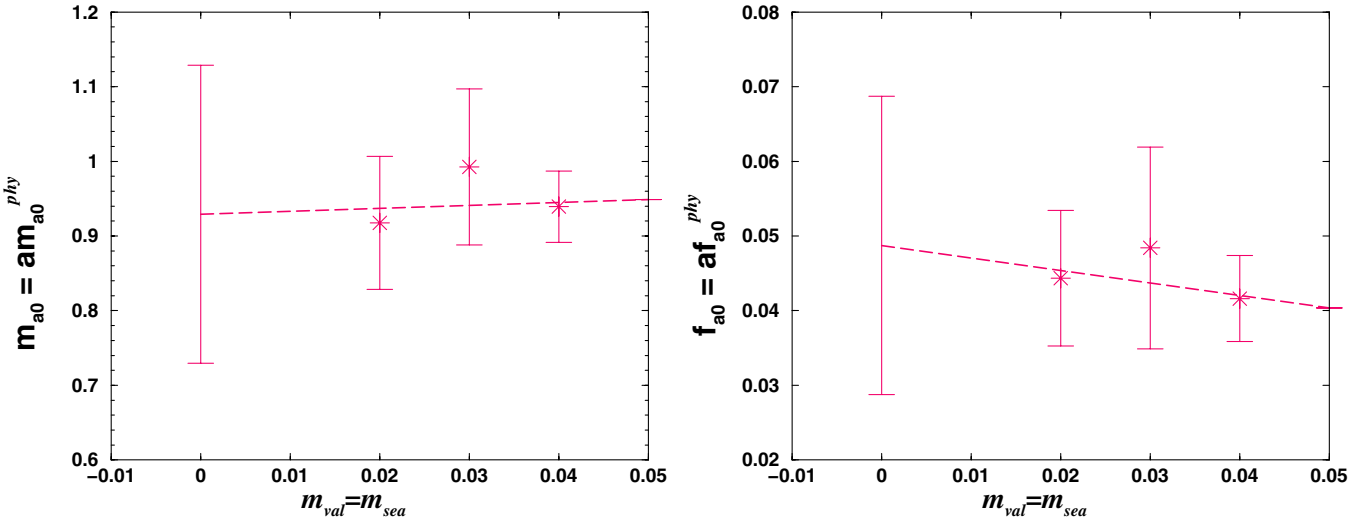

FIG. 2 (color online). The asterisks represent the mass m_{a0} and decay constant f_{a0} in the lattice units at the dynamical point $m_{\mathrm{val}} = m_{\mathrm{sea}}$, which are obtained from the exponential fit of the scalar correlators. The dashed line and the value at $m_q = 0$ are obtained with the linear fit.

III. ANALYSIS OF DYNAMICAL CORRELATORS WITH $m_{\mathrm{val}} = m_{\mathrm{sea}}$

The mass m_{a0} and the unrenormalized decay constant f_{a0} can be extracted from the dynamical scalar correlators using the exponential fit in the conventional way. Indeed, we will verify that the additional contribution from the exchange of two pseudoscalar fields in PQChPT [Fig. 3(b) (below)] exactly vanishes for $m_{\mathrm{val}} = m_{\mathrm{sea}}$, $N_f = 2$, and $m_0 \to \infty$ (12), so the simple exponential fit is well justified. The extracted masses and decay constants are shown in Fig. 2, while Table II presents also the time ranges $t = t_{\mathrm{min}}$–t_{max} and χ^2 of the fit.[3] The uncorrelated fits[4] are used throughout this work and the error bars are obtained using the jackknife method. The linear extrapolation to the chiral limit $m_{\mathrm{val}} = m_{\mathrm{sea}} \to 0$ gives results in lattice units[5]

$$m_{a0} = 0.93(20), \qquad f_{a0} = 0.049(20), \tag{2}$$

where the jackknife error bars are calculated as described in Appendix B of [19].

[3] t_{min} is taken throughout this work high enough so that there is no visible effect of the excited states and at the same time as low as possible in order to avoid large statistical errors. The choice of t_{max} has a negligible effect on the result and we take it at the time slice just before the signal is lost.

[4] We do not use the correlated fit with full covariance matrix in χ^2, since the number of configurations is quite small. A rather poor statistics is manifested by the fact that the results of uncorrelated and correlated fit do not agree very well. The results of the uncorrelated fit are more stable against the variation of the time range in the fit.

[5] The difference between the chiral extrapolations $m_q \to 0$ and $m_q \to -m_{\mathrm{res}}$ is negligible due to the smallness of $m_{\mathrm{res}} \approx 0.0014$ [14].

The resulting errors are rather large, which motivates us to extract the mass also from the partially quenched data with $m_{\mathrm{val}} \neq m_{\mathrm{sea}}$. This forces us to understand the effect of partial quenching in the following sections. The use of the partially quenched ChPT is crucial for this purpose since it enables us to subtract the significant partially quenched artifacts from the negative lattice correlators in the case of $m_{\mathrm{val}} < m_{\mathrm{sea}}$.

IV. SCALAR CORRELATOR IN PARTIALLY QUENCHED CHPT

In this section, we derive the nonsinglet scalar correlator in the partially quenched ChPT (PQChPT) within the so-called p-expansion regime. We consider the theory with N_{val} valence quarks q_i (which can have different masses m_i) and N_f degenerate sea quarks q_S of mass m_{sea}. The theory incorporates also N_{val} valence ghost quarks $\tilde{q}_i$ of mass m_i, which cancel the closed valence-quark loops. PQChPT enables us to study the partially quenched artifacts, which arise if the valence and the sea-quark masses are not equal and if $N_f \neq N_{\mathrm{val}}$. Our few lowest quark masses are low enough that $M_\pi^2/(4\pi f)^2 \ll 1$, while they

TABLE II. The m_{a0} and f_{a0} in lattice units obtained from the exponential fit to the dynamical correlators with $m_{\mathrm{val}} = m_{\mathrm{sea}}$. Time ranges $t = t_{\mathrm{min}}$–t_{max}, χ^2, and degrees of freedom (dof) in the fit are also shown.

$m_{\mathrm{val}} = m_{\mathrm{sea}}$	m_{a0}	f_{a0}	t	χ^2	dof
0.02	0.92(9)	0.044(9)	4–10	0.1	5
0.03	0.99(10)	0.048(13)	5–10	0.8	4
0.04	0.94(5)	0.042(6)	5–12	0.2	6

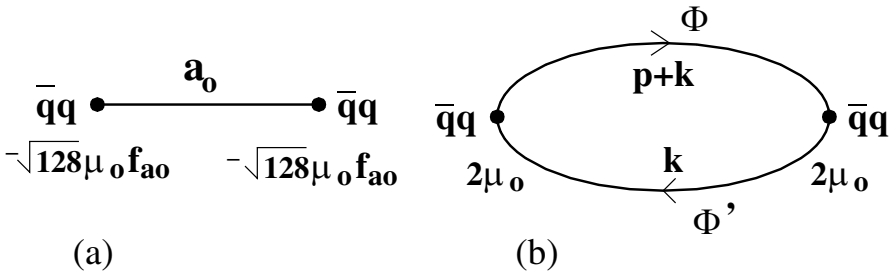

FIG. 3. The contributions to the nonsinglet scalar correlator in PQChPT: (a) the exchange of the scalar meson a_0; (b) the bubble diagram is responsible for the unphysical effect of partial quenching and represents the exchange of two pseudoscalar fields $\Phi\Phi'$. The intermediate pseudoscalar fields Φ and Φ' can have the flavor structure $\Phi, \Phi' \sim \bar{q}_i q_j, \bar{q}_i \tilde{q}_j, \bar{\tilde{q}}_i q_j, \bar{q}_i q_S, \bar{q}_S q_i$, where $q_{i,j}$ are the valence quarks and q_S the sea quark.

are still large enough that $M_\pi L \gg 1$ and we do not enter the ϵ regime on our lattice.

Nonphysical contributions to the scalar correlator in PQChPT arise from the exchange of pseudoscalar fields between the $\bar{q}q$ source and the $\bar{q}q$ sink. The leading contribution in the chiral expansion comes from the exchange of two pseudoscalar fields and is represented by the so-called *bubble diagram* in Fig. 3(b). The two pseudoscalar fields Φ and Φ' can be mesons $\Phi_{ij} \sim \bar{q}_i q_j$ and $\Phi_{iS} \sim \bar{q}_i q_S$ with boson statistics, or mesons $\Phi_{i\tilde{j}} \sim \bar{q}_i \tilde{q}_j$ with fermionic statistics. We do not consider the next-to-leading chiral corrections in PQChPT, which are suppressed by $\mathcal{O}[M_\pi^2/(4\pi f)^2]$ in comparison to the bubble diagram.[6] The lattice correlators can be interpreted as a sum of the a_0 exchange at the tree level in Fig. 3(a) and the bubble diagram in Fig. 3(b).

For our purpose, we need the strong interactions of pseudoscalar fields in PQChPT [15] as well as the kinetic and the mass term for the a_0 field[7]

$$\mathcal{L} = \frac{f^2}{4}\mathrm{str}[\partial^\mu U \partial_\mu U^\dagger] + f^2\mu_0 \mathrm{str}[\mathcal{M}^\dagger U + U^\dagger \mathcal{M}] - \frac{m_0^2}{6}(\mathrm{str}\Phi)^2 + \partial^\mu a_0 \partial_\mu a_0^\dagger - m_{a0}^2 a_0 a_0^\dagger, \tag{3}$$

with the physical values $f \sim 95$ MeV and three-flavor $m_0 \sim 600$–1000 MeV [20]. The field $U = \exp[\sqrt{2}i\Phi/f]$ incorporates the $\mathrm{SU}(N_{\mathrm{val}} + N_f|N_{\mathrm{val}})_L \times \mathrm{SU}(N_{\mathrm{val}} + N_f|N_{\mathrm{val}})_R$ Goldstone field matrix Φ. The quark mass matrix $\mathcal{M}$ is

$$\mathcal{M} = \mathrm{diag}(m_1, \ldots, m_{N_{\mathrm{val}}}, \underbrace{m_{\mathrm{sea}}, \ldots, m_{\mathrm{sea}}}_{N_f}, m_1, \ldots, m_{N_{\mathrm{val}}}),$$

and the supertrace is defined as $\mathrm{str}A = \sum_a \epsilon_a A_a$ with $\epsilon_a = 1$ for quarks and $\epsilon_a = -1$ for ghost quarks. The parameter μ_0 represents the slope of M_π^2 versus m_q and the pseudoscalar masses M are given by

$$M_{ab}^2 = 2\mu_0(m_a + m_b), \qquad a, b = i, \tilde{i}, S, \quad i = 1, .., N_{\mathrm{val}}, \qquad S = 1, .., N_f. \tag{4}$$

As is standard, we neglect the $\alpha(\partial \mathrm{str}\Phi)^2$ term in the Lagrangian since α seems to be small [9,20]. We also need the coupling of the a_0 field and the pseudoscalar fields to the nonsinglet scalar current[8]

$$\bar{q}_2 q_1 \sim -\mu_0 f^2 (U + U^\dagger)_{12} - \sqrt{128}\mu_0 f_{a0} a_0, \tag{5}$$

where f_{a0} plays the role of the scalar meson decay constant with the same normalization as in [8]

$$\langle 0|\bar{q}_2 q_1|a_0\rangle = -\sqrt{128}\mu_0 f_{a0}.$$

The point-point scalar correlator with external momentum $p = (\vec{0}, E)$,

$$C^{\mathrm{lat}}(t) \equiv \sum_{\vec{x}} \langle 0|\bar{q}_2(\vec{x}, t) q_1(\vec{x}, t) \bar{q}_1(\vec{0}, 0) q_2(\vec{0}, 0)|0\rangle, \tag{6}$$

is computed on the lattice and can be related to the prediction of PQChPT:

$$C^{\mathrm{PQChPT}}(t) = \mathrm{F.T.}\left[\frac{128\mu_0^2 f_{a0}^2}{p^2 + m_{a0}^2}\right] + B(t). \quad \downarrow \text{ continuum} \quad \frac{128\mu_0^2 f_{a0}^2}{2m_{a0}}(e^{-m_{a0}t} + e^{-m_{a0}(N_T - t)}) \tag{7}$$

The first term is the conventional a_0 exchange, while the second term $B(t) = \mathrm{FT}[B(p)]$ represents the contribution

[6]The next-to-leading order (NLO) chiral corrections were taken into account for fully quenched scalar correlator by resummation [8–10]. They are more complicated in partially quenched theory because partially quenched theory implies several intermediate states $\Phi\Phi'$ in Fig. 3(b), while quenched theory implies a single intermediate state $\pi\eta'$.

[7]A similar Lagrangian was used for the case of fully quenched ChPT in [8–10]. There μ_0 is denoted by $\frac{1}{2}r_0$.

[8]Similar current was used for the case of fully quenched ChPT in [8]. There μ_0 is denoted by $\frac{1}{2}r_0$.

of the bubble diagram in Fig. 3(b). The lattice Euclidean momenta $p = 2\sin(p_E/2)$ and the discrete Fourier transform (FT) on p_E are used when we compare PQChPT predictions (7) with the lattice correlators.[9] The bubble diagram is calculated from the Lagrangian (3) and the current (5) in Appendix A, giving

$$B(p) = 4\mu_0^2 \sum_k \Bigg\{ N_f \frac{1}{(k+p)^2 + M_{1S}^2} \frac{1}{k^2 + M_{2S}^2} - \frac{1}{N_f} \times \frac{1}{(k+p)^2 + M_{12}^2} \frac{k^2 + M_{SS}^2}{1 + \frac{k^2 + M_{SS}^2}{N_f m_0^2/3}} \Bigg[\frac{1}{(k^2 + M_{11}^2)^2} + \frac{1}{(k^2 + M_{22}^2)^2} + \frac{2}{(k^2 + M_{11}^2)(k^2 + M_{22}^2)} \Bigg] \Bigg\}. \quad (8)$$

Here k denotes the momenta in the loop [Fig. 3(b)] and the sum is performed over the allowed loop momenta in the finite box of the lattice. We use the lattice Euclidean momenta $k = 2\sin(k_E/2)$ and $k + p = 2\sin[(k_E + p_E)/2]$ when comparing the PQChPT prediction (7) with the lattice correlators. The detailed expression for $C^{\mathrm{PQChPT}}(t)$ used in the case of our finite lattice is presented in Appendix B.

We note that the contribution of the bubble diagram (8) has no unknown parameters, since one can fix the values of M, μ_0, and m_0 from other considerations. We determine the pseudoscalar meson masses M and $\mu_0 = M^2/(4m_q)$ from pion correlators on the same lattices. The hairpin insertion $m_0 \sim 600$–1000 MeV (normalized for three-flavors) has been determined from the η' correlator in a number of references [20], but the exact value of m_0 is not essential for the present work since the extracted scalar mass is almost independent of m_0 in the wide range $m_0 = [600\ \mathrm{MeV}, \infty]$ as will be demonstrated below.

In order to understand the effect of the bubble contribution on the lattice correlators, we derive the asymptotic form of $B(t)$ at large t for a correlator with $\vec{p} = 0$ on a lattice with $a \to 0$, $aN_T \to \infty$, and finite aN_L. The asymptotic form for degenerate valence quarks with mass m_{val} is

$$B(t) \overset{t\to\infty}{\to} \frac{2\mu_0^2}{N_L^3} \Bigg[\frac{e^{-2M_{VS}t}}{M_{VS}^2} \frac{N_f}{2} + \frac{e^{-(M_{VV}+M_{\eta'})t}}{M_{VV} M_{\eta'}} \frac{2N_f m_0^4}{9(M_{\eta'}^2 - M_{VV}^2)^2} + \frac{e^{-2M_{VV}t}}{M_{VV}^2} \frac{m_0^2}{3M_{VV}^2} \times \Bigg\{ -\frac{(M_{VV}^2 - M_{SS}^2)^2 + 1/3 N_f m_0^2 (M_{VV}^2 + M_{SS}^2)}{(M_{\eta'}^2 - M_{VV}^2)^2} + \frac{M_{VV}^2 - M_{SS}^2}{M_{\eta'}^2 - M_{VV}^2} M_{VV} t \Bigg\} \Bigg], \quad (9)$$

where $M_{\eta'}^2 \equiv M_{SS}^2 + \frac{1}{3} N_f m_0^2$ denotes η' mass in a theory with N_f flavors. We have assumed $M_{\eta'} > M_{VV}$ in derivation of (9), which is satisfied for the pseudoscalar masses of physical interest. The asymptotic behavior is dominated by a pair of zero-momentum pseudoscalar fields with mass $M_{VV} = 4\mu_0 m_{\mathrm{val}}$, a pair with mass $M_{VS} = 2\mu_0(m_{\mathrm{val}} + m_{\mathrm{sea}})$, or a pair with masses M_{VV} and $M_{\eta'}$. The dominant contribution at large t for $m_{\mathrm{val}} > m_{\mathrm{sea}}$ is proportional to $e^{-2M_{VS}t}$ and has positive sign. The dominant contribution for $m_{\mathrm{val}} < m_{\mathrm{sea}}$ is proportional to $t \cdot e^{-2M_{VV}t}$ and has negative sign given by $M_{VV}^2 - M_{SS}^2$. The bubble contribution is inversely proportional to the spatial volume of the lattice, so the effect of the bubble contribution is much less important for larger lattices. We summarize these findings which apply[10] for any values of N_f and m_0 as follows.

The scalar correlator receives a positive contribution $e^{-m_{a0}t}$ from the exchange of the a_0 meson and an additional bubble contribution from the exchange of two pseudoscalar fields $\Phi_1\Phi_2$. The bubble contribution is proportional to $e^{-(M_1+M_2)t}/N_L^3$ at large t and it is positive for $m_{\mathrm{val}} \geq m_{\mathrm{sea}}$ and negative for $m_{\mathrm{val}} < m_{\mathrm{sea}}$. The scalar correlator with $m_{\mathrm{val}} < m_{\mathrm{sea}}$ has a negative sign at large t if the bubble contribution dominates over the a_0 exchange. The bubble contribution is particularly important on lattices with smaller spatial volume if $M_1 + M_2 < m_{a0}$. The magnitude of the bubble contribution is predicted by PQChPT (8), which enables us to extract m_{a0} and f_{a0} by fitting the scalar correlators to PQChPT prediction (7).

We close this section by demonstrating that the analytical expressions for the bubble contribution (8) and (9) reduce to the known expressions in the fully quenched and the fully unquenched limits:

(i) The fully quenched ChPT corresponds to the limit $m_{\mathrm{sea}} \to \infty$ or equivalently to the limit $N_f \to 0$. Equations (8) and (9) reduce in this limit to

$$B^{\mathrm{QChPT}}(p) = -16\mu_0^2 \sum_k \frac{1}{(k+p)^2 + M^2} \times \frac{m_0^2/3}{(k^2 + M^2)^2}, \quad (10)$$

$$B^{\mathrm{QChPT}}(t) \overset{t\to\infty}{\to} -\frac{2\mu_0^2}{N_L^3} \frac{m_0^2}{3M^2} (1 + Mt) \frac{e^{-2Mt}}{M^2}, \quad (11)$$

with $M \equiv M_{VV}$ for degenerate valence quarks. Expression (10) agrees with the fully quenched expressions used in [8–10].[11]

(ii) In the case of full ChPT with SU(N_f) flavor symmetry $m_1 = m_2 = m_{\mathrm{sea}}$, the expressions (8) and (9) reduce to

[9] When we refer to conventional "exponential fit," we extract m_{a0} and f_{a0} from the fit to the first term in (7) using $p = 2\sin(p_E/2)$ and the discrete FT.

[10] These findings apply as long as the condition $M_{\eta'} > M_{VV}$ is satisfied, which was assumed in the derivation of (9).

[11] The $m_0^2/3$ can be viewed as the hairpin insertion in the quenched theory with one valence flavor, while $\mu_0 \equiv \frac{1}{2} r_0$ in [8–10].

$$B^{\mathrm{ChPT}}(p) = 4\mu_0^2 \frac{N_f^2 - 4}{N_f} \sum_k \frac{1}{(k+p)^2 + M^2} \times \frac{1}{k^2 + M^2} \overset{N_f=2}{\longrightarrow} 0 \quad \text{for } m_0 \to \infty, \tag{12}$$

$$B^{\mathrm{ChPT}}(t) \overset{t\to\infty}{\longrightarrow} \frac{\mu_0^2}{N_L^3 N_f}\left[4\frac{e^{-(M+M_{\eta'})t}}{M M_{\eta'}} + (N_f^2 - 4) \times \frac{e^{-2Mt}}{M^2}\right] \quad \text{for general } m_0, \tag{13}$$

where $M \equiv M_{VV} = M_{SS}$. This is in agreement with the conventional ChPT result. Bose symmetry and conservation of isospin allow only one intermediate state $\pi\eta'$ in $N_f = 2$ ChPT and this intermediate state gives a vanishing contribution in the $m_0 \to \infty$ limit. There are three intermediate states $\pi\eta$, $K\bar{K}$, and $\pi\eta'$ in $N_f = 3$ ChPT.

V. ANALYSIS OF LATTICE CORRELATORS USING PQCHPT

Our scalar correlators (6) are calculated in the partially quenched lattice QCD for $N_f = 2$ degenerate sea quarks with mass $m_{\mathrm{sea}} = 0.02$–0.04 and degenerate valence quarks with mass $m_{\mathrm{val}} = 0.01$–0.05 (Table I). In this section, we fit the lattice correlators to the one-loop prediction of the PQChPT given in Eq. (7). The PQChPT prediction is the sum of the a_0-exchange diagram and the bubble diagram (Fig. 3). The magnitude of the bubble contribution (8) is completely determined for a given choice of m_0 since we determine the values of M and μ_0 from the pseudoscalar correlators on the same configurations:

(i) The pseudoscalar masses are given by $M_{ab}^2 = \frac{1}{2}(M_{aa}^2 + M_{bb}^2)$, where M_{aa} is determined from the pseudoscalar correlator with $m_{\mathrm{val}} = m_a$ and the sea-quark mass of interest. The M_π from our lattice correlators are listed in Table III and shown in Fig. 4.

(ii) We fix $\mu_0 = M_{\mathrm{val,val}}^2/(4m_{\mathrm{val}})$ for given m_{val} and m_{sea}, where m_{res} is neglected[12] since it is much smaller than either m_{val} or m_{sea}. Here m_{val} is the input bare mass of the valence quark. $M_{\mathrm{val,val}}$ is the mass of the pion with two valence quarks of mass m_{val} at m_{sea} of interest.

The bubble diagram vanishes in the case of the dynamical theory ($m_{\mathrm{val}} = m_{\mathrm{sea}}$) with $N_f = 2$ and $m_0 \to \infty$ (12). In this case, the lattice correlator is interpreted solely by the a_0 exchange (7), it has exponential time dependence, and the corresponding m_{a0} was extracted in Sec. III. The bubble diagram is nonzero in general, so it has to be taken into account when the lattice correlators are fitted by Eq. (7) in order to extract m_{a0} and f_{a0}. The bubble contribution incorporates the physical contributions from the exchange of two pseudoscalars and also the unphysical effects of partial quenching when $m_{\mathrm{val}} \neq m_{\mathrm{sea}}$.

We note that our scalar correlators and the quark masses, used to determine $\mu_0 = M^2/(4m_q)$, are not renormalized. We would like to emphasize that this does not prevent us from extracting the physical mass m_{a0}. This can be seen by rearranging Eqs. (6) and (7):

$$m_q^2 \sum_{\vec{x}} \langle 0|\bar{q}_2 q_1(\vec{x},t)\bar{q}_1 q_2(\vec{0},0)|0\rangle = \mathrm{coef}\cdot(e^{-m_{a0}t} + e^{-m_{a0}(N_T - t)}) + \mathrm{FT}\left[\frac{M_\pi^4}{16}\frac{B(p)}{\mu_0^2}\right]. \tag{14}$$

TABLE III. The pion mass M_π in the lattice units, which is obtained from the fit to the pseudoscalar correlators at various m_{sea} and m_{val}.

m_{sea}	m_{val}	M_π	t	χ^2	dof
0.02	0.01	0.222(3)	8–15	0.4	6
0.02	0.02	0.294(2)	8–15	0.06	6
0.02	0.03	0.353(2)	8–15	0.02	6
0.02	0.04	0.405(2)	8–15	0.03	6
0.02	0.05	0.453(2)	8–15	0.07	6
0.03	0.02	0.304(2)	8–15	0.2	6
0.03	0.03	0.362(2)	8–15	0.05	6
0.03	0.04	0.412(2)	8–15	0.02	6
0.04	0.04	0.408(2)	8–15	0.4	6

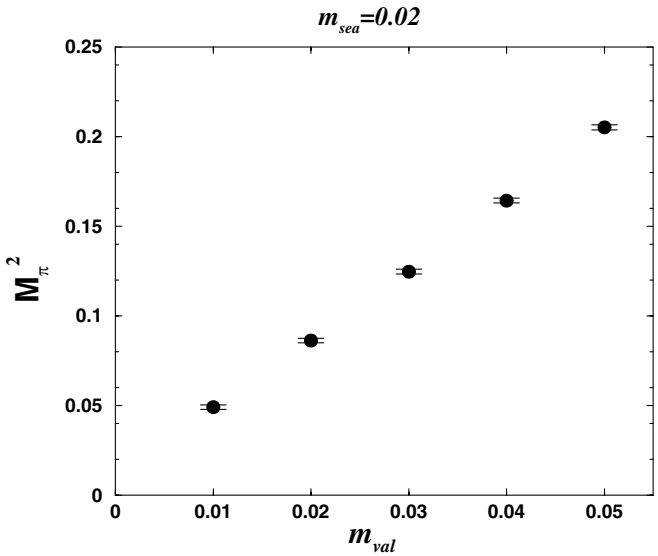

FIG. 4. $M_\pi^2(m_{\mathrm{val}})$ at $m_{\mathrm{sea}} = 0.02$ in lattice units.

[12]We have verified that the inclusion of the m_{res} in the PQChPT analysis has a negligible effect on the scalar masses. The resulting scalar masses which are obtained including m_{res} are well within the ranges given by the error bars on the scalar masses.

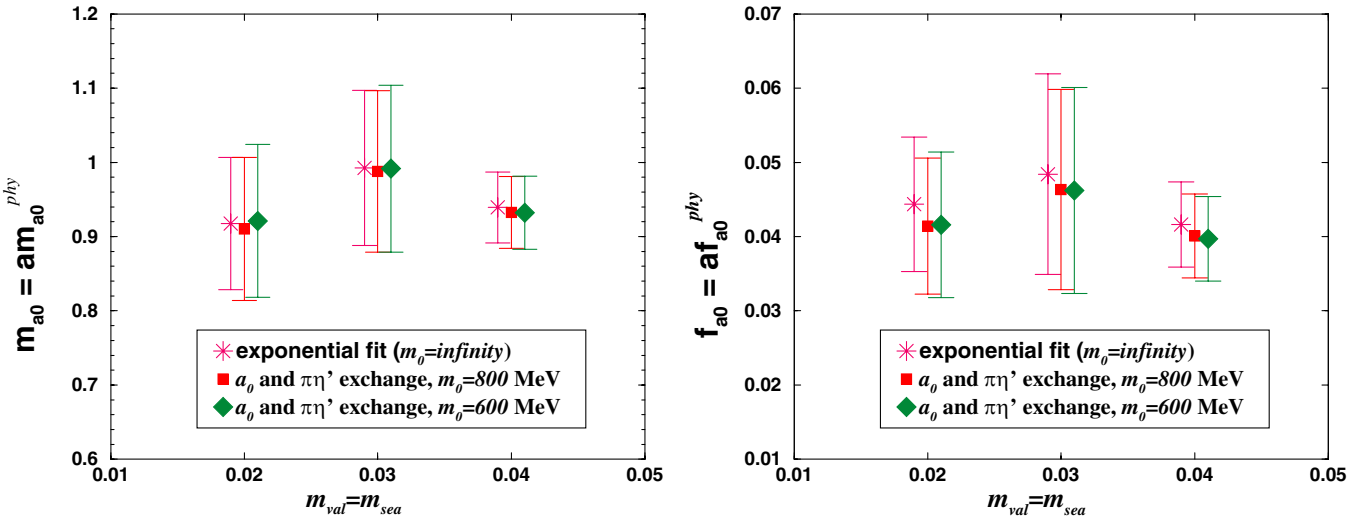

FIG. 5 (color online). The m_{a0} and f_{a0} in lattice units obtained from the fit of the dynamical scalar correlators with the PQChPT prediction (7) for various m_0. The PQChPT prediction for two-flavor dynamical correlators incorporates a_0 and $\pi\eta'$ exchange. The asterisks represent the fit for $m_0 \to \infty$, when the contribution from the $\pi\eta'$ state vanishes and the fit reduces to the standard exponential fit (asterisks are the same as asterisks in Fig. 2). The different data points are slightly shifted from $m_q = 0.02, 0.03, 0.04$ in the horizontal direction for clarity.

The product of quark mass and the scalar current $m_q\bar{q}q$ is invariant under renormalization. The second term on the right-hand side (rhs) of (14) depends only on the hadron masses M_π and m_0, which are also invariant under renormalization. The scalar mass m_{a0} can be therefore extracted from the first term on rhs without ambiguity from the renormalization.

A. Analysis of dynamical correlators taking into account $\pi\eta'$ intermediate state

The two-flavor dynamical scalar correlator receives a contribution from the exchange of a_0 and from the exchange of $\pi\eta'$. The contribution from the $\pi\eta'$ state vanishes in the limit $m_0 \to \infty$ and the fit reduces to the standard exponential fit used in Sec. III. The contribution of the $\pi\eta'$ intermediate state at finite m_0 is given by the bubble contribution (8) with $m_{\rm val} = m_{\rm sea}$ and $N_f = 2$. The fit of the dynamical correlators to PQChPT prediction (7) at various m_0 gives m_{a0} and f_{a0} in Fig. 5. The results are almost independent of m_0 and agree with the result of the conventional exponential fit in Sec. III. For this reason, we will refer to Sec. III for our dynamical results in the conclusions.

The extracted m_{a0} and f_{a0} are almost insensitive to the presence of the $\pi\eta'$ state since the contribution of this state is at least an order of magnitude smaller than the dynamical lattice correlators in the fitted time range for $m_0 \geq 600$ MeV. Our dynamical correlators are dominated by the a_0 exchange although the mass $M_\pi + M_{\eta'} = M_\pi + (M_\pi^2 + 2/3m_0^2)^{1/2}$ is comparable to the mass m_{a0} in Table II. This can be attributed to our spacial volume 16^3 which is large enough to suppress the contribution $e^{-(M_\pi+M_{\eta'})t}/N_L^3$ of the $\pi\eta'$ exchange in Eq. (13).

B. Analysis of the partially quenched correlators with $m_{\rm val} \neq m_{\rm sea}$

Our analysis of the partially quenched correlators is based on the correlators with $m_{\rm sea} = 0.02$ since a range of $m_{\rm val} = 0.01$–0.05 is available only in this case (see Table I).

The lattice correlators (1) and the PQChPT bubble contribution $B(t)$ (7) and (8) are compared in Fig. 6 for $m_{\rm sea} = 0.02$ and various $m_{\rm val}$. The PQChPT predictions in Figs. 6(b) and 6(c) show just the bubble contribution without the a_0-exchange contribution in order to indicate the importance of the bubble contribution for various $m_{\rm val}$ at fixed $m_{\rm sea}$. Figure 6 exhibits good qualitative agreement between the lattice correlators and the PQChPT predictions at various $m_{\rm val}$:

(i) The lattice correlator and the bubble contribution are both negative and large for $m_{\rm val} < m_{\rm sea}$ due to a striking unphysical effect of partial quenching. The bubble contribution is large and negative for $m_{\rm val} = 0.01$ since it falls like $-t \cdot e^{-2M_{VV}t}$ at large t (9), where the corresponding pion mass $M_{VV} = 0.222(3)$ is small (Table III).

(ii) The dynamical lattice correlator with $m_{\rm val} = m_{\rm sea}$ is positive. The bubble contribution describes the exchange of physical $\pi\eta'$ and vanishes in the limit $m_0 \to \infty$ (12).

(iii) The lattice correlator at $m_{\rm val} > m_{\rm sea}$ is positive and receives a positive and rather small contribution from the bubble, which is less and less important for larger $m_{\rm val}$. The bubble contribution is positive and relatively small since it falls as a linear combination of $+e^{-2M_{VS}t}$ and $+t \cdot e^{-2M_{VV}t}$ at large t (9), where the pseudoscalar masses M_{VS} and M_{VV}

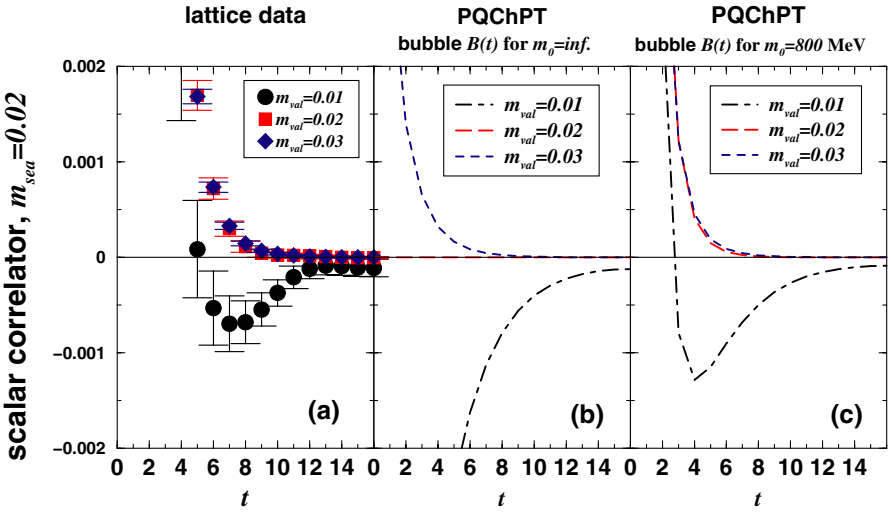

FIG. 6 (color online). The scalar correlator for $m_{\text{sea}} = 0.02$ and various m_{val}: the lattice data (a) and the bubble contribution $B(t)$ as predicted by PQChPT for $m_0 \to \infty$ (b) and $m_0 \to 800$ MeV (c). The PQChPT prediction (7) in this figure represents just $B(t)$ and does not contain the contribution from the a_0 exchange.

are relatively large for $m_{\text{val}} \geq 0.03$ and $m_{\text{sea}} = 0.02$.

While we do not include it in the extraction of our final results, we have a limited set of partially quenched data for the $m_{\text{sea}} = 0.03$ evolution, and we have checked that the lattice correlators change sign at $m_{\text{val}} = m_{\text{sea}}$ also in this case. This can be seen in Fig. 1(b).

Let us have a closer look at the case of $m_{\text{val}} = 0.01$ and $m_{\text{sea}} = 0.02$ in Fig. 7, where the effect of partial quenching is most striking. The bubble contribution (dot-dashed line) is in good quantitative agreement with the data for $t \geq 8$, where the a_0 exchange fades exponentially. The exchange of the a_0 scalar meson is dominant at smaller t.

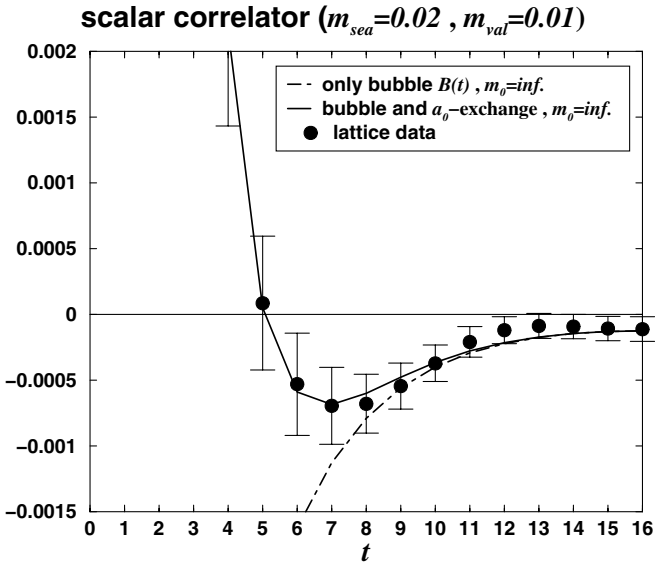

FIG. 7. The data and PQChPT predictions for the scalar correlator at $m_{\text{sea}} = 0.02$, $m_{\text{val}} = 0.01$, and $m_0 = \infty$.

The fit of the data to the PQChPT prediction (7) gives $m_{a0} = 0.87(17)$ and $f_{a0} = 0.040(15)$ at $m_0 \to \infty$. The PQChPT prediction with this choice of m_{a0} and f_{a0} is given by the solid line in Fig. 7 and describes the lattice correlator well. Our one-loop analytical formula therefore correctly determines the sign and approximate size of the effects when the valence-quark mass is lower than the sea-quark mass. This gives us confidence in the veracity of applying this formula to the larger valence-quark masses, where the loop effects are smaller.

All scalar correlators for $m_{\text{sea}} = 0.02$ and various m_{val} are fitted by the PQChPT prediction (7), and the resulting m_{a0} and f_{a0} are given in Fig. 8 and Table IV. Figures on the left represent the fit, which incorporates both the bubble and the a_0-exchange contributions. We find that m_{a0} and f_{a0} at $m_{\text{val}} \geq 0.02$ depend very slightly on the hairpin insertion m_0 in the range $m_0 = [600\ \text{MeV}, \infty]$. In the case of $m_{\text{val}} = 0.01$, the central values of m_{a0} and f_{a0} depend significantly on m_0, but they are all consistent for m_0 in the range $[600\ \text{MeV}, \infty]$ within the large error bars.[13] The result of the linear extrapolation from $m_{\text{val}} = 0.01$–0.05 to the chiral limit $m_{\text{val}} \to 0$ is practically independent of whether the $m_{\text{val}} = 0.01$ data is taken into account due to the large error bars at $m_{\text{val}} = 0.01$ with current statistics. The linear extrapolation from $m_{\text{val}} = 0.01$–0.05 gives

[13]Large error bars on m_{a0} and f_{a0} at $m_{\text{val}} = 0.01$ arise since they are obtained from the fit to the difference of the lattice correlator and the bubble contribution. The lattice correlator and the bubble contribution are negative and large for $m_{\text{val}} = 0.01$, so their difference is small and has a relatively large error bar.

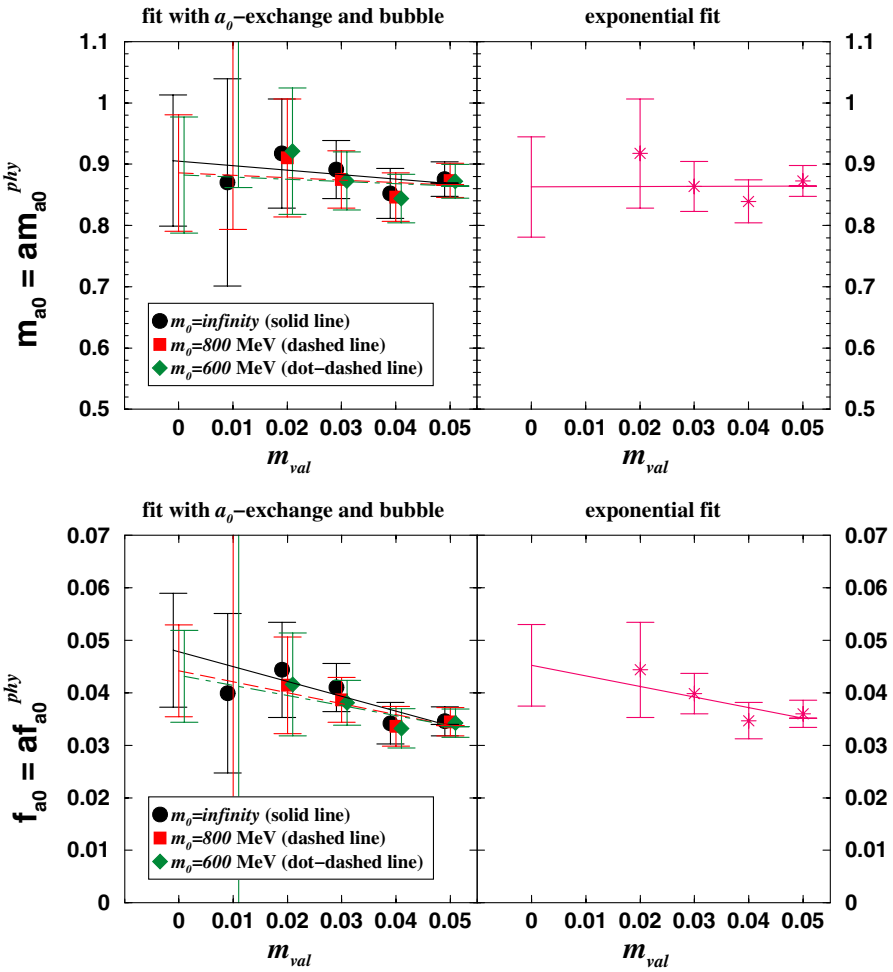

FIG. 8 (color online). The m_{a0} and f_{a0} in lattice units obtained from the fit of the scalar correlators at $m_{\rm sea} = 0.02$ with the PQChPT prediction (7). The left figures represent the fit results, when the bubble contribution is taken into account and m_0 is varied. The right figures represent the conventional exponential fit $e^{-m_{a0}t} + e^{-m_{a0}(N_T-t)}$, which is obtained under the assumption that the bubble contribution vanishes; the correlator with $m_{\rm val} = 0.01$ and $m_{\rm sea} = 0.02$ is negative and cannot be described by $e^{-m_{a0}t} + e^{-m_{a0}(N_T-t)}$. The different data points are slightly shifted in the horizontal direction for clarity.

$$\begin{aligned} m_{a0} &= 0.90(11), \quad f_{a0} = 0.048(11) \quad \text{for } m_0 \to \infty, \\ m_{a0} &= 0.89(9), \quad f_{a0} = 0.044(9) \quad \text{for } m_0 = 800\text{MeV}, \\ m_{a0} &= 0.88(9), \quad f_{a0} = 0.043(9) \quad \text{for } m_0 = 600\ \text{MeV}, \end{aligned} \tag{15}$$

which are consistent for $m_0 = [600\ \text{MeV}, \infty]$. So the chiral extrapolation $m_{\rm val} \to 0$ at fixed $m_{\rm sea} = 0.02$ leads to the mass in the lattice units

$$m_{a0} = 0.89(11), \tag{16}$$

where the error reflects the statistical error of the data and the variation of the bubble contribution for m_0 in the range $m_0 = [600\ \text{MeV}, \infty]$.

The conventional exponential fit of the scalar correlators for $m_{\rm val} \geq m_{\rm sea} = 0.02$ gives m_{a0} and f_{a0} in Fig. 8 on the right. The bubble contribution in Eq. (7) is taken to be zero in this case. The exponential fit obviously does not work for the correlator at $m_{\rm val} = 0.01$, where the intriguing partially quenched artifact has to be incorporated through the bubble contribution. However, it gives reasonable m_{a0} and f_{a0} for $m_{\rm val} \geq m_{\rm sea}$: The results from the exponential fit are consistent with the results from the fit to Eq. (7) since the bubble contribution is zero or relatively small for $m_{\rm val} \geq m_{\rm sea}$.

VI. NONSINGLET SCALAR MESON MASS

In this section we collect our main results on the scalar meson mass.

The chiral extrapolation $m_q \to 0$ of the two-flavor *dynamical* data points $m_{\rm val} = m_{\rm sea} = m_q$ gives [Eq. (2)]

$$m_{a0} = 0.93 \pm 0.20 \quad \text{or} \quad m_{a0}^{\rm phy} = 1.58 \pm 0.34\ \text{GeV}, \tag{17}$$

where only the statistical error is given. The number in

TABLE IV. The m_{a0} and f_{a0} in lattice units obtained from the fit of the correlators with the PQChPT prediction (7) at $m_{\rm sea} = 0.02$ and various $m_{\rm val}$. The fits denoted by "bubble and a_0 exchange" take into account both terms in Eq. (7). The bubble contribution in (7) depends on the value of m_0, which is taken to be $m_0 = 600$ MeV, 800 MeV, ∞. We also present the results of the conventional exponential fit $e^{-m_{a0}t} + e^{-m_{a0}(N_T-t)}$, which is obtained under the assumption that the bubble contribution vanishes; the correlator with $m_{\rm val} < m_{\rm sea}$ is negative (Fig. 1) and cannot be described by $e^{-m_{a0}t} + e^{-m_{a0}(N_T-t)}$.

$m_{\rm val}$	Type of fit to Eq. (7)	m_0 [MeV]	m_{a0}	f_{a0}	t	χ^2	dof
	Exponential fit						
0.01	Bubble and a_0 exchange	∞	0.87(17)	0.040(15)	4–8	0.2	3
	Bubble and a_0 exchange	800	1.2(5)	0.077(70)		1.2	
	Bubble and a_0 exchange	600	1.8(9)	0.19(30)		3.0	
	Exponential fit		0.92(9)	0.044(9)		0.1	
0.02	Bubble and a_0 exchange	∞	0.92(9)	0.044(9)	4–10	0.1	5
	Bubble and a_0 exchange	800	0.91(10)	0.041(9)		0.1	
	Bubble and a_0 exchange	600	0.92(10)	0.042(10)		0.1	
	Exponential fit		0.86(4)	0.040(4)		3.0	
0.03	Bubble and a_0 exchange	∞	0.89(5)	0.041(5)	4–11	2.0	6
	Bubble and a_0 exchange	800	0.87(5)	0.039(4)		1.8	
	Bubble and a_0 exchange	600	0.87(5)	0.038(4)		1.8	
	Exponential fit		0.84(4)	0.035(3)		1.4	
0.04	Bubble and a_0 exchange	∞	0.85(4)	0.034(4)	5–12	1.0	6
	Bubble and a_0 exchange	800	0.85(4)	0.033(4)		0.9	
	Bubble and a_0 exchange	600	0.84(4)	0.033(4)		0.9	
	Exponential fit		0.87(3)	0.036(3)		1.9	
0.05	Bubble and a_0 exchange	∞	0.88(3)	0.034(3)	5–12	1.6	6
	Bubble and a_0 exchange	800	0.87(3)	0.034(3)		1.4	
	Bubble and a_0 exchange	600	0.87(3)	0.034(3)		1.4	

GeV is obtained using the preliminary result for the scale $a^{-1} \approx 1.7$ GeV [14].

We extracted also the scalar meson masses from the *partially quenched* correlators with $m_{\rm val} \neq m_{\rm sea}$. The chiral extrapolation $m_{\rm val} \to 0$ at fixed $m_{\rm sea} = 0.02$ leads to

$$m_{a0} = 0.89 \pm 0.11 \quad \text{or} \quad m_{a0}^{\rm phy} = 1.51 \pm 0.19\,\text{GeV}, \qquad (18)$$

and we expect that the dependence on the sea-quark mass is small. Here the error reflects the statistical error of the data and the variation of the bubble contribution for m_0 in the range $m_0 = [600\ \text{MeV}, \infty]$ [see Eq. (16) and Fig. 8].

The chiral limits of m_{a0} in the dynamical case and in the partially quenched case are consistent. Note that the error is smaller in the partially quenched case, where the application of the partially quenched ChPT was crucial. The mass of the simulated $q\bar{q}$ state is somewhat larger than the mass of $a_0(980)$ and it is closer to the mass of $a_0(1450)$. We note that our result is consistent with the fully quenched results of Refs. [8–10] within the present accuracy.[14]

[14]The fully quenched results of [8–10] are presented in the introduction and are consistent with (17) and (18) if the effect of quenching is incorporated at the leading order in the chiral expansion (one bubble). The quenched m_{a0} is somewhat lower if the quenching effect is incorporated at the next-to-leading order [10].

Finally we comment on the scalar isodoublet mesons $s\bar{u}$ and $s\bar{d}$, since their relation to the controversial resonance κ is still an open question. We are not able to make a reliable estimate for the mass of the $s\bar{u}$ and $s\bar{d}$ scalar mesons, since we did not simulate nondegenerate valence quarks. We get a rough estimate by extrapolating the mass obtained from the dynamical correlators to $\frac{1}{2}(m_s + m_{u,d})$. The resulting mass $m_\kappa \sim 0.92(9)$ or $m_\kappa^{\rm phy} \sim 1.6 \pm 0.2$ GeV seems higher than the mass of the reported experimental candidate ($\sim$800 MeV [5]) although the interpretation of this observation as κ is controversial.

VII. CONCLUSIONS

We presented a lattice study of the lightest scalar $q\bar{q}$ state with nonsinglet flavor structure (a_0 meson). Good chiral properties of the domain wall fermions are important for the connected scalar correlator since this is the first step toward a controlled investigation of the scalar spectrum, in particular the σ particle, which is intimately related to the chiral symmetry breaking. Two degenerate sea quarks were simulated with masses corresponding to $M_\pi \sim 500$–700 MeV. The simulations were done at fixed lattice spacing and one size of the volume.

The value of scalar mass $m_{a0} = 0.93 \pm 0.20$ in the lattice units was extracted in the conventional way from the dynamical correlators ($m_{\rm val} = m_{\rm sea}$) and the resulting

error is rather large. The corresponding physical mass $m_{a0}^{\rm phy} = 1.58 \pm 0.34$ GeV was obtained using the preliminary result for the scale $a^{-1} \approx 1.7$ GeV.

We analyzed also the partially quenched correlators with $m_{\rm val} \neq m_{\rm sea}$. They exhibit a striking effect of partial quenching since they are positive for $m_{\rm val} \geq m_{\rm sea}$ and negative for $m_{\rm val} < m_{\rm sea}$ (Fig. 1). In order to understand this effect of partial quenching, we derived the scalar correlator within the partially quenched ChPT. The leading unphysical contribution comes from the exchange of two pseudoscalar fields and has no unknown parameters. We have shown that this contribution is positive for $m_{\rm val} \geq m_{\rm sea}$, it is negative for $m_{\rm val} < m_{\rm sea}$, and it is inversely proportional to spatial volume at large time separations. The physical contribution to the scalar correlator is due to the exchange of the scalar meson a_0 and has conventional exponential time dependence. We find that the sum of these two contributions describes our partially quenched lattice correlators very well. We extract the mass $m_{a0} = 0.89 \pm 0.11$ or $m_{a0}^{\rm phy} = 1.51 \pm 0.19$ GeV from partially quenched correlators, which is consistent with the mass extracted from our dynamical correlators.

Our current simulation of the $q\bar{q}$ state on the lattice seems to indicate that this state is somewhat heavier than the observed resonance $a_0(980)$, and it is closer to the observed resonance $a_0(1450)$; however, given the size of our errors this is not conclusive. We must also emphasize that we have only two dynamical flavors, our lattice volume is not very large, and also our quark masses are quite heavy. Besides, continuum limit has not been taken as we have data at only one lattice spacing, so the exploratory nature of our study needs to be kept in mind.

We also note that the $N_f = 2$ theory is likely to have interesting differences from QCD ($N_f = 2 + 1$). Recall that the observed resonances $a_0(980)$ and $a_0(1450)$ decay to $\eta\pi$ and $K\bar{K}$. Bose statistics and isospin conservation restrict $a_o^{N_f=2} \not\to \pi + \pi$ for $N_f = 2$, though $a_0^{N_f=2} \to \eta'^{N_f=2} + \pi$ would be possible if kinematics allows it. Additional intricacy could be also caused by the presence of a large four-quark component in these channels. Thus, the approach to the chiral limit may well exhibit a more involved dependence of the scalar mass on the quark mass than our data (see Fig. 2) indicates with relatively heavy quarks. These issues will need to be addressed in future works with more computing resources.

ACKNOWLEDGMENTS

The dynamical domain wall fermion configurations were generated by the RBC Collaboration and were essential for the lattice results in the present paper. It is a pleasure to thank all the members of the RBC Collaboration, in particular, Tom Blum, Yasumichi Aoki, Norman Christ, Bob Mawhinney, Shigemi Ohta, and June Noaki. We also thank RIKEN, Brookhaven National Laboratory, and U.S. Department of Energy for providing the facilities essential for the completion of this work. All computations were carried out on the QCDSP supercomputers at the RIKEN-BNL Research Center and at Columbia University. The research of A. S. was supported in part by USDOE Contract No. DE-AC02-98CH10886. K. O. was supported in part by DOE Grant No. DFFC02-94ER40818.

APPENDIX A: CALCULATION OF THE BUBBLE DIAGRAM

In this appendix we derive the result $B(p)$ [Eq. (8)] for the bubble diagram in Fig. 3(b). The coupling of the nonsinglet scalar current and two pseudoscalar fields Φ is given by Eq. (5):

$$\bar{q}_2 q_1 = 2\mu_0 (\Phi^2)_{12}. \tag{19}$$

The scalar correlator receives the following contribution from the exchange of the two pseudoscalar fields shown in Fig. 3(b):

$$B = \langle 0|\bar{q}_2 q_1 \bar{q}_1 q_2|0\rangle_{\rm bubble} = 4\mu_0^2 \langle 0|\Phi_{1a}\Phi_{a2}\Phi_{2b}\Phi_{b1}|0\rangle, \tag{20}$$

where indices a and b are summed over all quarks and ghost quarks of the partially quenched theory: $a, b = i, \tilde{i}, S$ with $i = 1, \ldots, N_{\rm val}$ and $S = 1, \ldots, N_f$. The nonzero Wick contractions relevant to the diagram on the Fig. 3(b) are

$$\begin{aligned} B = 4\mu_0^2 (&\langle\Phi_{1S}|\Phi_{S1}\rangle\langle\Phi_{S2}|\Phi_{2S}\rangle + \langle\Phi_{1i}|\Phi_{i1}\rangle\langle\Phi_{i2}|\Phi_{2i}\rangle \\ &+ \langle\Phi_{1\tilde{i}}|\Phi_{\tilde{i}1}\rangle\langle\Phi_{\tilde{i}2}|\Phi_{2\tilde{i}}\rangle + \langle\Phi_{11}|\Phi_{22}\rangle\langle\Phi_{12}|\Phi_{21}\rangle \\ &+ \langle\Phi_{22}|\Phi_{11}\rangle\langle\Phi_{12}|\Phi_{21}\rangle). \end{aligned} \tag{21}$$

The propagators for the pseudoscalar fields follow from the Lagrangian (3). The propagator for the flavor nondiagonal mesons ($a \neq b$) in Minkowski space is

$$\langle\Phi_{ab}|\Phi_{ba}\rangle = i\frac{\delta_{ab}\epsilon_a}{p^2 - M_{aa}^2}, \tag{22}$$

while for the diagonal mesons the propagator is [15]

$$\begin{aligned} \langle\Phi_{aa}|\Phi_{bb}\rangle = i\Bigg[&\frac{\delta_{ab}\epsilon_a}{p^2 - M_{aa}^2} - \frac{1}{N_f}\frac{p^2 - M_{SS}^2}{(p^2 - M_{aa}^2)(p^2 - M_{bb}^2)} \\ &\times \frac{1}{1 - \frac{p^2 - M_{SS}^2}{N_f m_0^2/3}}\Bigg]. \end{aligned} \tag{23}$$

The analytical expression [Eq. (8)] for the bubble diagram in Fig. 3 is obtained by inserting the propagators (22) and (23) to the expression (21) and by performing the Wick rotation to the Euclidean space.

APPENDIX B: PQCHPT CORRELATOR FOR A FINITE LATTICE

The PQChPT prediction for the scalar correlator $C^{\mathrm{PQChPT}}(t)$ (7) relevant for a finite lattice of the volume $N_L^3 N_T$ is

$$C^{\mathrm{PQChPT}}(t) = \frac{1}{N_T}\sum_{m_4=-N_T/2}^{N_T/2-1}\cos\left(\frac{2\pi m_4}{N_T}t\right)\left(\frac{128\mu_0^2 f_{a0}^2}{[2\sin(\frac{1}{2}\frac{2\pi m_4}{N_T})]^2+m_{a0}^2}+4\mu_0^2\frac{1}{N_L^3 N_T}\sum_{n_{1,2,3}=-N_L/2}^{N_L/2-1}\sum_{n_4=-N_T/2}^{N_T/2-1}\left\{N_f\frac{1}{(k+p)^2+M_{1S}^2}\right.\right.$$
$$\left.\left.\times\frac{1}{k^2+M_{2S}^2}-\frac{1}{N_f}\frac{1}{(k+p)^2+M_{12}^2}\frac{k^2+M_{SS}^2}{1+\frac{k^2+M_{SS}^2}{N_f m_0^2/3}}\left[\frac{1}{(k^2+M_{11}^2)^2}+\frac{1}{(k^2+M_{22}^2)^2}+\frac{2}{(k^2+M_{11}^2)(k^2+M_{22}^2)}\right]\right\}\right), \tag{24}$$

with

$$k^2=\sum_{i=1}^{3}[2\sin\left(\frac{1}{2}\frac{2\pi n_i}{N_L}\right)]^2+\left[2\sin\left(\frac{1}{2}\frac{2\pi n_4}{N_T}\right)\right]^2,\qquad (k+p)^2=\sum_{i=1}^{3}\left[2\sin\left(\frac{1}{2}\frac{2\pi n_i}{N_L}\right)\right]^2+\left[2\sin\left(\frac{1}{2}\left\{\frac{2\pi n_4}{N_T}+\frac{2\pi m_4}{N_T}\right\}\right)\right]^2. \tag{25}$$

The notation is given in Sec. IV. This correlator is compared with the lattice correlators $C^{\mathrm{lat}}(t)$ (6) in Sec. V.

[1] See, for example, F. E. Close and N. A. Tornqvist, J. Phys. G **28**, R249 (2002).
[2] Particle Data Group, K. Hagiwara *et al.*, Phys. Rev. D **66**, 010001 (2002).
[3] W. Lee and D. Weingarten, Phys. Rev. D **61**, 014015 (2000).
[4] E791 Collaboration, E. M. Aitala *et al.*, Phys. Rev. Lett. **86**, 770 (2001).
[5] D.V. Bugg, Phys. Lett. B **518**, 47 (2001); E791 Collaboration, E. M. Aitala *et al.*, Phys. Rev. Lett. **89**, 121801 (2002); BES Collaboration, J. Z. Bai *et al.*, hep-ex/0304001.
[6] M. G. Alford and R. L. Jaffe, Nucl. Phys. **B578**, 367 (2000); AIP Conf. Proc. **688**, 208 (2004).
[7] D. Kaplan, Phys. Lett. B **288**, 342 (1992); V. Furman and Y. Shamir, Nucl. Phys. **B439**, 54 (1995); T. Blum and A. Soni, Phys. Rev. D **56**, 174 (1997); Phys. Rev. Lett. **79**, 3595 (1997);CP-PACS Collaboration, A. Ali Khan *et al.* , Phys. Rev. D **63**, 114504 (2001); RBC Collaboration, T. Blum *et al.*, Phys. Rev. D **69**, 074502 (2004); RBC Collaboration, T. Blum *et al.*, Phys. Rev. D **66**, 014504 (2002).
[8] W. Bardeen, A. Duncan, E. Eichten, N. Isgur, and H. Thacker, Phys. Rev. D **65**, 014509 (2002).
[9] W. Bardeen, E. Eichten, and H. Thacker, Phys. Rev. D **69**, 054502 (2004).
[10] RBC Collaboration, S. Prelovsek and K. Orginos, Nucl. Phys. Proc. Suppl. **B119**, 822 (2003).
[11] SCALAR Collaboration, T. Kunihiro *et al.*, Phys. Rev. D **70**, 034504 (2004); see also SCALAR Collaboration, T. Kunihiro *et al.*, Nucl. Phys. Proc. Suppl. **119**, 275 (2003); **129**, 242 (2004).
[12] C. McNeile and C. Michael, Phys. Rev. D **63**, 114503 (2001); A. Hart, C. McNeile, and C. Michael, Nucl. Phys. Proc. Suppl. **119**, 266 (2003).
[13] MILC Collaboration, C. Bernard *et al.*, Phys. Rev. D **64**, 054506 (2001); MILC Collaboration, C. Aubin *et al.*, hep-lat/0402030.
[14] RBC Collaboration, C. Dawson *et al.*, Nucl. Phys. Proc. Suppl. **128**, 54 (2004); **129**, 167 (2004); RBC Collaboration, T. Izubuchi *et al.*, Nucl. Phys. Proc. Suppl. **B119**, 813 (2003); RBC Collaboration, T. Blum *et al.*, BNL-HET-04/11; RBRC-426; CU-TP-1115, KANAZAWA-04-14, hep-lat/0411006.
[15] C. Bernard and M. Golterman, Phys. Rev. D **49**, 486 (1994); S. Sharpe, Phys. Rev. D **56**, 7052 (1997); S. Sharpe and N. Shoresh, Phys. Rev. D **62**, 094503 (2000); Phys. Rev. D **64**, 114510 (2001).
[16] RBC Collaboration, Y. Aoki *et al.*, Phys. Rev. D **69**, 074504 (2004).
[17] S. Necco, Nucl. Phys. **B683**, 137 (2004).
[18] Y. Kuramashi *et al.*, Phys. Rev. Lett. **72**, 3448 (1994).
[19] CP-PACS Collaboration, A. A. Khan *et al.*, Phys. Rev. D **65**, 054505 (2002).
[20] See, for example, H. Witting, Nucl. Phys. Proc. Suppl. **B119**, 59 (2003), and references therein.